JOURNAL OF GUIDANCE, CONTROL, AND DYNAMICS
Vol. 28, No. 6, November–December 2005

Bank-to-Turn Missile Guidance with Radar Imaging Constraints

Asif Farooq*
MBDA UK, Ltd., Stevenage, England SG1 2DA, United Kingdom
and
David J. N. Limebeer†
Imperial College, London, England SW7 2BT, United Kingdom

The problem of optimizing the trajectory for an air-to-surface missile using bank-to-turn steering is addressed. The missile uses a radar imaging seeker to detect targets. A cruise missile scenario is considered that is characterized by low-level flight, followed by a climb and dive onto the target (a "bunt" trajectory). The use of a radar imaging seeker imposes constraints on the missile's trajectory, and these constraints must be made an integral part of any optimization problem. Examples are presented that show that the launch crossrange offset, terminal angle constraints, and the constraints associated with Doppler beam sharpening radars all have a strong influence on the optimal controls. These results provide useful insight into the flight trajectories of these missiles and the way in which they might be implemented.

Nomenclature

A_h, A_v	=	horizontal and vertical acceleration demands, ms^{-2}
A_{mx}, A_{my}, A_{mz}	=	accelerations achieved (body axes), ms^{-2}
A'_{my}, A'_{mz}	=	accelerations sensed at accelerometers (body axes), ms^{-2}
A_{yd}, A_{zd}	=	acceleration demands (yaw and pitch, respectively), ms^{-2}
a_0, a_1, a_2	=	coefficients for air density polynomial, $\mathrm{kg}\cdot\mathrm{m}^{-3}$, $\mathrm{kg}\cdot\mathrm{m}^{-4}$, and $\mathrm{kg}\cdot\mathrm{m}^{-5}$, respectively
b_0, b_1, b_2	=	coefficients for sonic speed polynomial, ms^{-1}, s^{-1}, and $\mathrm{m}^{-1}\mathrm{s}^{-1}$, respectively
C_{lp}, $C_{l\delta}$, $C_{l\beta}$	=	roll stability derivatives, rad^{-1}
C_{m0}, $C_{m\delta}$, $C_{m\alpha}$, C_{mq}	=	pitch stability derivatives, rad^{-1}
C_{nr}, $C_{n\delta}$, $C_{n\beta}$	=	yaw stability derivatives, rad^{-1}
C_x, C_y, C_z	=	aerodynamic coefficients
C_{x0}, $C_{x\alpha}$	=	axial stability derivatives, rad^{-1}
$C_{y\beta}$, $C_{y\delta}$	=	body sideforce stability derivatives, rad^{-1}
C_{z0}, $C_{z\alpha}$, $C_{z\delta}$	=	body lift force stability derivatives, rad^{-1}
$c(\cdot)$	=	cosine of angle
c_t, c_h	=	scaling factors for performance index
d	=	distance from accelerometer to center of gravity in body x axis, m
d_0, d_1, d_2, d_3, d_4, d_5	=	coefficients for Doppler beam sharpening (DBS) angle profiling function
F_x, F_y, F_z	=	aerodynamic forces in body axes, N
f	=	function for desired DBS angle behavior
g	=	acceleration due to gravity, ms^{-2}
I_{xx}, I_{yy}, I_{zz}	=	roll, pitch, and yaw moment of inertias, $\mathrm{kg}\cdot\mathrm{m}^2$
I_{xz}	=	product of inertia, $\mathrm{kg}\cdot\mathrm{m}^2$
J	=	performance index
K_{1p}, K_{2p}, K_{3p}, K_{4p}	=	pitch autopilot gains
K_{1y}, K_{2y}, K_{3y}, K_{4y}	=	yaw autopilot gains
$K_{1\phi}$, K_{1r}	=	roll autopilot gains
k	=	parabolic drag coefficient
$\bar{L}$, $\bar{M}$, $\bar{N}$	=	external moments, $\mathrm{N}\cdot\mathrm{m}$
l_r	=	reference length, m
M_n	=	Mach number
m	=	missile mass, kg
N	=	number of discretization intervals
p, q, r	=	roll, pitch, and yaw rates, deg/s
p_{dem}, q_{dem}, r_{dem}	=	rate demands for autopilot loops, deg/s
p_i	=	piecewise constant function
p_0, p_1, p_2, p_3, p_4	=	coefficients for acceleration demand initial guess polynomial
Q	=	dynamic pressure, $\mathrm{kgm}^{-1}\mathrm{s}^{-2}$
R	=	range to go, m
R_{sx}, R_{sy}, R_{sz}	=	downrange, crossrange, and altitude, respectively, m
$R_{sx}(t_f)$, $R_{sy}(t_f)$, $R_{sz}(t_f)$	=	target coordinates, m
r_0, r_1, r_2	=	coefficients for roll demand initial guess polynomial
S	=	reference area, m^2
SFC	=	specific fuel consumption, $\mathrm{kg}/(\mathrm{N}\cdot\mathrm{s})$
S_s	=	speed of sound, ms^{-1}
$s(\cdot)$	=	sine of angle
T	=	applied thrust, N
T_{dem}	=	demanded thrust, N
t, t_f	=	current time and final times, respectively, s
U, V, W	=	velocity components in body axes, ms^{-1}
V_{sx}, V_{sy}, V_{sz}	=	inertial space frame components of the velocity vector, ms^{-1}
V'_{sx}, V'_{sy}, V'_{sz}	=	unit velocity components in inertial axes
V_t	=	total missile speed, ms^{-1}
x_o, y_o, z_o	=	target offset in downrange, crossrange, and altitude, m
x_p, y_p	=	pitch and yaw autopilot integrator outputs, rad

Received 9 July 2004; revision received 1 December 2004; accepted for publication 13 December 2004.

*Senior Engineer, Advanced Studies Department, Seeker Division; asif.farooq@mbda.co.uk.

†Professor and Head, Department of Electrical and Electronic Engineering; d.limebeer@imperial.ac.uk.

x_s, y_s, z_s = unit sightline vector components in inertial axes
x_{sw}, y_{sw}, z_{sw} = unit sightline vector components in velocity axes
α, β = angles of incidence and sideslip, respectively, deg
γ, χ = flight path and heading angle, respectively, deg
Δ = crossrange resolution, m
$\delta_p, \delta_q, \delta_r$ = fin angle demands, rad
$\delta'_p, \delta'_q, \delta'_r$ = fin angles achieved, rad
δt = DBS integration period, s
ϵ = throttle setting
Θ = seeker pitch gimbal angle, deg
Θ_T = total angle between velocity and sightline, deg
θ, ψ, ϕ = pitch, yaw, and roll angles, respectively, deg
λ = wavelength, m
Ξ, Λ = DBS angles in azimuth and elevation, respectively, deg
ρ = air density, $\mathrm{kg} \cdot \mathrm{m}^{-3}$
τ = roll autopilot rate loop time constant, s
Φ = seeker roll gimbal angle, deg
ϕ_d = roll autopilot demand, deg

I. Introduction

CURRENT air-to-surface cruise missiles use both global positioning systems (GPS) and an inertial navigation system (INS) to navigate to a designated target. A terrain database is prestored in the missile flight computer, and the missile will fly at low altitudes to evade detection by air defense units. A typical cruise missile will also fly through designated waypoints for route planning purposes. During midcourse guidance, a combination of GPS, INS, and terrain stored data are blended in the guidance command calculations. For enhanced lethality, some missions require a climb and dive on to the target in the terminal phase (a "bunt" trajectory). In these cases the missile will "pop up" in altitude at a designated range to go. During the terminal climb, a seeker is used to acquire the target, and the guidance laws are designed to achieve a required impact angle and miss distance.

Recently, there has been interest in the use of radar imaging for precision guidance. Fine resolution in downrange can be achieved using short transmitted pulses or pulse compression techniques, and improved crossrange resolution can be accomplished using Doppler beam sharpening (DBS) processing. When DBS is used, a radar image of the terrain is generated and is continually updated during flight. The radar image is used to identify features of the terrain, locate targets, and, finally, to select an aimpoint on the target. DBS exploits the fact that within a single range resolution cell scatterers have different Doppler shifts (due to different angular offsets), which can be resolved using Doppler filtering. The pulse returns in each range bin are stored over the DBS integration period, corrected for phase deviations using the INS (autofocusing), and then summed and transformed into a radar image using Doppler filtering. Further details on DBS signal processing can be found in Refs. 1 and 2. We consider the geometric constraints that radar imaging imposes on the missile trajectory when bank-to-turn (BTT) steering is used. For crossrange resolution purposes, DBS imposes a constraint on the missile flight path, which needs to be offset in azimuth angle from the sightline vector. The exact angular offset required depends on a number of factors, including the missile speed, mechanical/airframe limits, and the DBS integration period.

For DBS radars, conventional guidance methods such as proportional navigation are inappropriate because they do not address the need to maintain a velocity component perpendicular to the sightline vector. A transverse velocity component is critical for the successful implementation of DBS because this induces the differential Doppler shift required to resolve scatterers in crossrange. It is not possible to both image and home in on the target for the whole engagement. One method of resolving this conflict is to use DBS for target recognition and aimpoint selection and to transfer from DBS mode to real-beam monopulse for final terminal guidance, for example, over the last 2 km. This approach requires the correlation of the real beam and the final radar image from handover to impact. The seeker then extracts the angular errors from the range/Doppler cells and uses an angle tracking filter to derive sightline rate estimates. Another possible technique is to employ DBS up to a very short range (of approximately 500 m) while tracking a selected aimpoint on the DBS image.

Following a brief summary of previous research, the missile model is developed in Sec. II. The model uses linearized aerodynamics and contains autopilot loops, actuators, standard atmospheric data and an engine model. It is based on a six-degree-of-freedom (six-DOF) representation of a BTT airframe. It is usually necessary to simplify the complex dynamic model for optimization purposes, and methods for doing this are described. To validate the optimal control laws, they are fed into the full six-DOF model as reference autopilot inputs, and the output trajectories are compared with those of the simplified model.

In Sec. III, the problem requirements, some of which are conflicting, are translated into an optimal control problem. Because the equations of motion are nonlinear, analytic means of solving these optimization problems are difficult to apply, and recourse to numerical optimization is, therefore, necessary. The infinite dimensional optimal control problem can be converted into a finite dimensional parameter optimization problem via a discretization scheme. The resulting problem can then be solved using a nonlinear programming technique such as sequential quadratic programming. An optimal control toolbox based on the algorithms described in Ref. 3 is used for the numerical computations. The methodology is further explained in Sec. III, and the results are presented in Sec. IV. The results are then discussed and a number of conclusions drawn.

In a previous paper,[4] a similar problem was investigated for an airframe using skid-to-turn (STT) steering. In this study, a simplified (quadratic) model of the missile airframe and autopilot closed loop was used. A 5-km initial crossrange offset was imposed, and optimal trajectories, which fulfilled the various mission constraints, were generated. This paper augments this previous study by investigating the use of BTT control methods. BTT trajectories for DBS radars have not been reported on in the open literature, and this paper investigates some of the guidance issues associated with this problem. The use of BTT guidance is motivated by the fact that a BTT missile can be designed to be lighter, stealthier, and more aerodynamically efficient (by exploiting higher lift-to-drag ratios). With BTT steering, the missile's lateral acceleration is achieved by rolling the missile body, thereby causing the aerodynamic lift vector to both counteract gravity and produce a sideforce. The optimization of BTT trajectories is a challenging problem because the controls and the airframe dynamics are coupled through the roll angle and the roll rate. BTT control and guidance logic and trajectory optimization have received considerable interest in the past decade, and it is worth briefly reviewing some of that work. Some of the practical issues associated with BTT missile guidance (as compared with STT guidance) are addressed in Ref. 5. The performance of various BTT steering laws is then discussed and evaluated. Autopilot design for BTT missiles using robust control has also been reported in Refs. 6–8. The use of polar converting logic is discussed in Ref. 9, and an alternative method based on the nonzero effort miss is proposed to compute guidance commands for a BTT missile.

Apart from the papers in the missile guidance field, there is a substantial body of research on trajectory optimization for related aerospace guidance problems. Previous research can be characterized as trajectory studies that analyze open-loop solutions and closed-loop guidance that addresses potential implementation schemes. For trajectory studies, most authors adopt simplified point-mass models, though there is some research on the use of higher-order body rate models for optimization.[10] Examples of BTT trajectory studies using numerical optimal control include

minimum-time-to-turn problems for fighter aircraft in Refs. 10 and 11 and low-altitude fly-to-point maneuvers in Ref. 12.

Various classical techniques for stabilization about a nominal trajectory are neighboring optimal control,[13] linear quadratic regulator,[14] and predictive control[15] methods. In Ref. 16, trajectory tracking for unmanned air vehicles (UAV) is considered. Reference trajectories are specified in an inertial frame, and robust control theory is used to design a sequence of linear controllers to track trimming trajectories. In Ref. 17, an approximate receding horizon control law is used to track reference trajectories for a reentry guidance problem. In contrast to traditional approaches, the method formulates the tracking problem as a linear time-varying stabilization problem, and a receding horizon control law is proposed that stabilizes the system over a finite horizon. If tracking a single nominal trajectory is seen as limiting, methods such as those investigated in Ref. 18 are applicable. Here, a whole field of extremals is stored, and neural networks are used to interpolate the optimal controls. The application in this paper is for a hypersonic launch vehicle with a potential elevon failure.

An alternative method of implementing optimal trajectories is to solve the (nonlinear) optimal control problem repeatedly online, using the optimal controls as inputs in a guidance scheme. In this case, the repeated update of the optimal controls generates a feedback mechanism. For aerospace systems, fast dynamics mean that the computational delay in arriving at an optimal solution cannot be ignored from a stability viewpoint. Of recent interest are the inverse dynamic methods that exploit system structure. In Ref. 19, differential flatness is used to reduce the dimensionality of the optimal control problem by searching for flat outputs and mapping these to the full state space. In aerospace problems, most practical systems are underactuated and have saturation limits, and so this technique is not easy to apply directly. An interesting solution to this is presented in Ref. 20, in which artificial pseudocontrols are introduced and maneuvers for an UAV are computed using this technique.

Terminal guidance for air-to-surface missiles with DBS radars is a relatively new research area reflecting that radar imaging sensors have not been proposed for missile guidance until very recently. In Ref. 21, DBS trajectories are parameterized using circular arcs, and an acceleration profile is derived from these parametric curves using a specific guidance law. An alternative approach to curve parameterization is to employ a trajectory optimization procedure. In Ref. 22, open-loop STT DBS trajectories are obtained using trajectory optimization of a point-mass model. The trajectories studied assume an initial altitude offset of 1 km and terminal approach angle constraints. A fixed crossrange resolution is specified as a path constraint, and the profile of the DBS trajectory is determined via this constraint. The open-loop optimal trajectories are then approximated by matching the closed-loop guidance law of Ref. 21 to the open-loop controls.

II. Model

The six-DOF model used in this study is based on a fin-controlled cruise missile. Most missiles have three autopilots for the roll, pitch, and yaw channels that generate the fin actuation signals internally. The deflections of the fins generate torques that rotate the missile airframe to achieve the commanded accelerations and roll angle command. Feedback of the achieved accelerations and the measured roll angle enables the missile to track the commanded signals. An overview of the missile system is shown in Fig. 1. Missiles generally employ either STT or BTT steering. The choice of steering law is dictated by a number of factors such as the airframe design, the propulsion system, and the type of sensors employed. In an STT missile, the desired pitch and yaw accelerations are computed in missile body axes from the guidance law, and the missile is stabilized in roll. For a BTT system two controls are used to steer the missile. The missile pitch plane (the xz plane in missile body axes) is rotated by the roll angle, and a total acceleration command in the pitch plane is specified and sent to the pitch autopilot (Fig. 2). As a result, a BTT steering law can be envisaged as generating an acceleration vector in the missile pitch plane, the magnitude of the vector being specified by the total acceleration command and its orientation (relative to inertial axes) specified by the roll angle. In a BTT system, the pitch and roll channels are principally used to guide the missile. Conventionally, closed-loop guidance is accomplished by calculating the horizontal and vertical acceleration demands A_h and A_v via the guidance law. A Cartesian-to-polar transformation coupled with BTT logic is used to convert these acceleration demands to equivalent BTT steering commands (total pitch acceleration A_{zd} and roll angle demand ϕ_d). The steering commands are then passed to the autopilot loops for implementation, resulting in an achieved pitch acceleration A_{mz} and roll angle ϕ (Fig. 2). Given the horizontal and vertical acceleration demands A_h and A_v, the choice of STT or BTT steering can be selected arbitrarily, and, in some scenarios, it may be preferable to use mixed steering to combine the advantages of both steering laws, provided that this is compatible with the airframe and engine requirements. Such an approach might be used in an anti-air context in which the advantages of STT (faster response time, smaller miss distance) could be combined with the extended range obtained using BTT steering. However, when computing open-loop optimal controls, the Cartesian-to-polar transformation cannot be

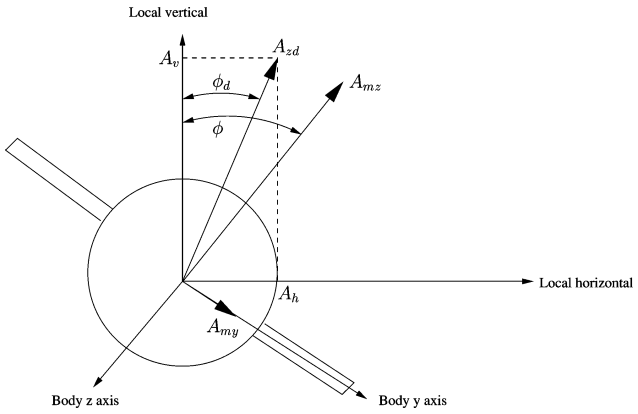

Fig. 2 BTT guidance.

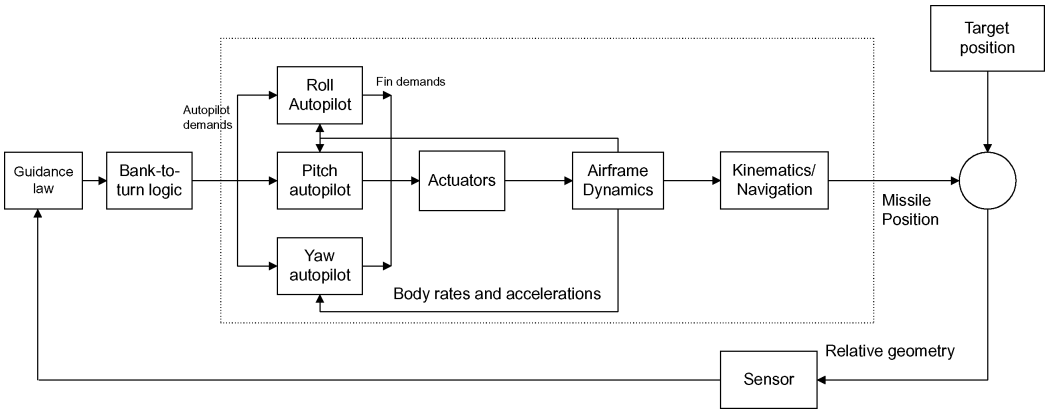

Fig. 1 Missile system.

used to select a steering law arbitrarily because the position states are required and the transformation matrix from missile body axes to inertial axes would be different for BTT or STT. It is possible to allow the optimizer choose the steering law. For instance, if the pitch, roll, and yaw demands are chosen as the controls then either BTT or STT, or a mixed strategy, could be selected. This presupposes an airframe that is capable of implementing either steering law. In this paper, BTT steering is assumed. The natural choice of control variables for this problem are the pitch and roll autopilot inputs (A_{zd} and ϕ_d in Fig. 2). An equally valid approach uses the Cartesian acceleration demands A_h and A_v, but this requires the use of complex BTT logic to generate the roll demand ϕ_d, and this logic cannot easily be implemented in an optimal control formulation. The outer guidance loop is cut, and reference commands are computed that are sent to each of the autopilots for implementation. (See Fig. 1, in which the dotted lines effectively represent the system without a guidance loop.) The autopilot dynamics are included in the model used for optimization. This provides a higher fidelity representation of the missile dynamics. The aerodynamic data are supplied at a particular reference flight condition. The main modeling assumptions are as follows:

1) The aerodynamic stability derivatives are constant throughout the flight.
2) The target coordinates are fixed and known in advance.
3) The seeker tracking dynamics are perfect.
4) The missile moves in a still air mass (wind is neglected).
5) INS and instrumentation errors are neglected.
6) The missile's main body product of inertia I_{xz} is neglected.
7) Maximum thrust is used throughout the terminal guidance phase.
8) The ground terrain is flat and level.

A. Vehicle Equations

The standard flight equations for a missile in body-fixed axes over a "flat Earth" are

$$m\dot{U} = F_x + T - mg\sin(\theta) - rV + qW \tag{1}$$

$$m\dot{V} = F_y + mg\sin(\phi)\cos(\theta) + pW - rU \tag{2}$$

$$m\dot{W} = F_z + mg\cos(\phi)\cos(\theta) + qU - pV \tag{3}$$

where F_x, F_y, and F_z are the aerodynamic forces. The gravitational force components are treated separately. The rotational dynamics are expressed as

$$\dot{p} = (\bar{L}/I_{xx}) - [(I_{zz} - I_{yy})/I_{xx}]qr \tag{4}$$

$$\dot{q} = (\bar{M}/I_{yy}) - [(I_{xx} - I_{zz})/I_{yy}]rp \tag{5}$$

$$\dot{r} = (\bar{N}/I_{zz}) - [(I_{yy} - I_{xx})/I_{zz}]pq \tag{6}$$

where $\bar{L}$, $\bar{M}$, and $\bar{N}$ are the external moments acting on the missile. The calculation of the aerodynamic forces and moments acting on the missile generally requires the use of lookup tables that are based on wind-tunnel data. For this study, we consider linearized aerodynamics, which are based on Taylor series expansions about a particular reference flight condition. For small angles of incidence, the aerodynamic lift force in body axes can be modeled as being linearly dependent on the angle of incidence and the fin deflection. Similarly, the sideforce is modeled to be linearly dependent on the sideslip angle and the rudder deflection. The drag is modeled as a quadratic function of incidence with a parasitic component. The drag due to the fin deflections is neglected. Given this, one obtains

$$F_x = QSC_x = QS\left[C_{x0} + (kC_{x\alpha})\alpha^2\right] \tag{7}$$

$$F_y = QSC_y = QS[C_{y\beta}\beta + (C_{y\delta})\delta_r'] \tag{8}$$

$$F_z = QSC_z = QS[C_{z0} + C_{z\alpha}\alpha + (C_{z\delta})\delta_q'] \tag{9}$$

in which the dynamic pressure is

$$Q = \rho V_t^2/2 = \rho(U^2 + V^2 + W^2)/2 \tag{10}$$

The aerodynamic moments are modeled as

$$\bar{L} = QSl_r[C_{l\beta}\beta + C_{lp}l_r p/V_t + (C_{l\delta})\delta_p'] \tag{11}$$

$$\bar{M} = QSl_r[C_{m0} + C_{m\alpha}\alpha + C_{mq}l_r q/V_t + (C_{m\delta})\delta_q'] \tag{12}$$

$$\bar{N} = QSl_r[C_{n\beta}\beta + C_{nr}l_r r/V_t + (C_{n\delta})\delta_r'] \tag{13}$$

The angles of incidence and sideslip can be calculated from the components of the velocity vector in body axes:

$$\alpha = \tan^{-1}(W/U) \tag{14}$$

$$\beta = \sin^{-1}(V/V_t) \tag{15}$$

For small angles, these functions can be approximated by the argument itself. For a BTT missile, it is desirable to keep the sideslip small, which implies $V \approx 0.0$. The speed of sound and air density vary with altitude. Tabulated data from the 1976 U.S. Standard Atmosphere model[23] were obtained at discrete altitudes up to a maximum altitude of 2500 m, and polynomials were used to approximate the air density ρ and sonic speed S_s as a function of altitude. The model equations were

$$\rho = a_0 + a_1 R_{sz} + a_2 R_{sz}^2 \tag{16}$$

$$S_s = b_0 + b_1 R_{sz} + b_2 R_{sz}^2 \tag{17}$$

where $a_0 = 1.225\ \text{kg}\cdot\text{m}^{-3}$, $a_1 = -1.1725 \times 10^{-4}\ \text{kg}\cdot\text{m}^{-4}$, $a_2 = 4.0162 \times 10^{-9}\ \text{kg}\cdot\text{m}^{-5}$, $b_0 = 340.3\ \text{ms}^{-1}$, $b_1 = -0.0038\ \text{s}^{-1}$, and $b_2 = -2.28 \times 10^{-8}\ \text{m}^{-1}\text{s}^{-1}$. Given the forces and moments, the missile orientation and position can be calculated via a set of kinematic equations. The Euler angles can be calculated as

$$\dot{\phi} = p + q\tan(\theta)\sin(\phi) + r\tan(\theta)\cos(\phi) \tag{18}$$

$$\dot{\theta} = q\cos(\phi) - r\sin(\phi) \tag{19}$$

$$\dot{\psi} = q[\sin(\phi)/\cos(\theta)] + r[\cos(\phi)/\cos(\theta)] \tag{20}$$

and the missile position in inertial axes is calculated as

$$\dot{R}_{sx} = V_{sx} \tag{21}$$

$$\dot{R}_{sy} = V_{sy} \tag{22}$$

$$\dot{R}_{sz} = V_{sz} \tag{23}$$

where

$$V_{sx} = U[c(\theta)c(\psi)] + V[s(\phi)s(\theta)c(\psi) - c(\phi)s(\psi)] + W[s(\phi)s(\psi) + c(\phi)s(\theta)c(\psi)] \tag{24}$$

$$V_{sy} = U[c(\theta)s(\psi)] + V[c(\phi)c(\psi) + s(\phi)s(\theta)s(\psi)] + W[c(\phi)s(\theta)s(\psi) - s(\phi)c(\psi)] \tag{25}$$

$$V_{sz} = U[s(\theta)] - V[s(\phi)c(\theta)] - W[c(\phi)c(\theta)] \tag{26}$$

in which $\cos(\cdot)$ and $\sin(\cdot)$ are abbreviated as $c(\cdot)$ and $s(\cdot)$, respectively, and positive altitude corresponds to a height above sea level. The flight path and the heading angles describe the orientation of the velocity vector with respect to inertial axes. These can be calculated from the inertial space velocity components as

$$\gamma = \sin^{-1}(V_{sz}/V_t) \tag{27}$$

$$\chi = \tan^{-1}(V_{sy}/V_{sx}) \tag{28}$$

B. Engine Model

The engine model represents spoolup delays and the effect of altitude on the maximum demanded thrust and is based on a (scaled) turbojet model. The maximum thrust at sea level and a number of discrete altitudes were used to inform the engine model. The thrust reduction with altitude is approximately linear for low (less than 2000-m) altitudes. The effect of the Mach number on the maximum thrust was neglected, and the maximum thrust is modeled as

$$T_{\text{dem}} = (4500 - 0.3R_{sz})\epsilon \tag{29}$$

The demanded thrust is multiplied by the throttle setting ϵ and passed through a lumped first-order lag (of 1 s). The applied thrust is then used in the dynamic equations. The engine dynamics are represented as a lumped first-order lag of 1 s:

$$\dot{T} = -T + T_{\text{dem}} \tag{30}$$

As the missile generates thrust by expending fuel, the mass of the missile reduces. The relevant equation for estimating the fuel flow is

$$\dot{m} = -(T)\text{SFC} \tag{31}$$

where SFC is the specific fuel consumption of the engine and the initial condition in Eq. (31) corresponds to the initial missile mass (1200 kg) at the start of terminal guidance. For the purposes of this study, the SFC was assumed to be constant.

C. Autopilot and Actuator Equations

The missile control is achieved via pitch, roll, and yaw autopilots that track reference commands. Most tactical missile autopilots are composed of an outer acceleration loop and an inner body-rate loop for the control of the pitch and yaw channels. For a BTT missile, the yaw channel is decoupled and given a zero reference, whereas the pitch acceleration demand and roll angle demand are the main control variables. The function of the autopilots is to provide good command following and disturbance rejection in the presence of modeling uncertainties, as well as generating the actuation signals necessary to track the reference command signals. For constant aerodynamic stability derivatives, fixed-gain autopilots can achieve a satisfactory tracking response. With varying stability derivatives, the autopilot would be gain scheduled, for example, as a function of Mach number. The trajectory optimization procedure can be extended to gain-scheduled autopilots using smooth interpolating functions. The autopilot should also be compensated for gravity and rolling motion. For brevity, the autopilot equations are merely stated with the loop gains being selected to provide a satisfactory tracking response. Without actuator dynamics, the pitch and yaw closed-loop autopilot responses can be shown to be equivalent to third-order transfer functions. Because the pitch and yaw autopilots contain an integrator in the forward loop, the internal dynamics for the acceleration autopilot loops can be modeled as follows:

$$\dot{x}_p = K_{1p}(A_{zd} - A'_{mz}) - K_{2p}[g\cos(\theta)\cos(\phi) + A'_{mz}] - K_{3p}(q) + K_{1\phi}(\phi_d - \phi)\beta \tag{32}$$

$$\dot{y}_p = K_{1y}(0 - A'_{my}) + K_{2y}[g\cos(\theta)\sin(\phi) + A'_{my}] - K_{3y}(r) + K_{1\phi}(\phi_d - \phi)\alpha \tag{33}$$

where A_{zd} and ϕ_d represent the pitch and roll demands, respectively. The tracking error signals are multiplied by gains K_{1p} and K_{1y}, and there is feedback of the body rates q and r and both roll and gravitational compensation. The roll compensation terms are functions of the angles of incidence and sideslip; these angles would have to be estimated from measured data. Note that although the yaw autopilot input is zero, the output may be nonzero. The yaw autopilot is used primarily to regulate the sideslip angle. Because the accelerometers are not placed at the center of gravity, the measured accelerations (A'_{my}, A'_{mz}) will differ from the accelerations at the center of mass (A_{my}, A_{mz}). These are related by the following moment arm terms:

$$A'_{my} = A_{my} + d(\dot{r}) \tag{34}$$

$$A'_{mz} = A_{mz} - d(\dot{q}) \tag{35}$$

where d is the axial distance between the accelerometer triad and the center of gravity in body axes. The fin angles are related to the autopilot states by

$$\delta_p = K_{1\phi}(\phi_d - \phi) - K_{1r}(p) \tag{36}$$

$$\delta_q = x_p - K_{4p}(q) \tag{37}$$

$$\delta_r = y_p - K_{4y}(r) \tag{38}$$

where $K_{1\phi}$, K_{1r}, K_{4p}, and K_{4y} are autopilot gains. The three autopilot output signals δ_p, δ_q, and δ_r have to be mixed before their application to the four aerodynamic control surfaces. (See Ref. 24 for the relevant equations.) The control surface actuators are modeled as second-order filters with angle (25 deg) and angle rate limits (500 deg/s). The achieved control surface signals are then recombined to generate the signals δ'_p, δ'_q, and δ'_r that are used in aerodynamic equations.

D. DBS and Gimbal Angle Equations

The gimbal angles Θ and Φ are defined as the angles between the missile antenna and body-fixed x axis, and the relevant equations for the inner pitch, outer roll gimbal mechanism assumed in this study can be found in Ref. 24. The main factor impacting on the crossrange resolution is the azimuth angle between the velocity and sightline vectors. Other factors that are, to some extent, controllable are the range, the missile speed, and the angle between the velocity and sightline in elevation. When coherent DBS processing is used, the crossrange resolution is given by (Ref. 4)

$$\Delta = \frac{R\lambda}{2V_t(\delta t)\sin(\Xi)\cos(\Lambda)} \tag{39}$$

From this equation, one sees that the azimuth DBS angle Ξ should be kept large to minimize the crossrange resolution. In the azimuth plane, this requires tight control of the missile velocity vector. In addition, the elevation DBS angle Λ should be kept small. A steep bunt requirement will lead to larger values of Λ and a higher speed drop that will degrade the crossrange resolution. The ideal DBS trajectory for imaging is a spiral toward the target, but this is not practical due to extended flight times, and so other methods of trajectory generation need to be considered. Table 1 shows the seeker parameters assumed for this study. See the Appendix for DBS angle derivation calculations.

E. Airframe Parameters

The airframe parameters used in this study are listed in Table 2. Whereas the mass varies with the fuel load, all of the other parameters are assumed to be constant.

F. Model Simplifications

To keep the optimal control computations manageable, the model used for computing the optimal controls was simplified. The full six-DOF model includes the presence of fast states such as roll rate and discontinuities such as saturation functions, and these can cause difficulties for the optimizer. In flight dynamics, it is well known that timescale separations exist. There are fast states associated with the body-rate dynamics and slower states corresponding to the position and velocity states. Most difficulty is associated with the roll rate

Table 1 DBS parameters

Parameter	Value
Transmit frequency, GHz	35
Wavelength, m	0.0085
Seeker coherent integration period δt, s	0.3, 0.4, 0.5

Table 2 Missile data

Parameter	Value
Initial mass m, kg	1200
Roll, pitch, and yaw inertia I_{xx}, I_{yy}, and I_{zz}, kg · m^2	60, 1500, 1600
Distance from accelerometer to center of gravity d, m	0.5
Parabolic drag coefficient k	5.0
Reference length l_r, m	0.63
Reference area S, m^2	0.3117
Axial derivatives C_{x0}, $C_{x\alpha}$, rad^{-1}	0.17, 0.69
Sideforce derivatives $C_{y\beta}$, $C_{y\delta}$, rad^{-1}	−22.92, −2.29
Normal force derivatives C_{z0}, $C_{z\alpha}$, $C_{z\delta}$, rad^{-1}	−0.39, −24.64, −2.64
Roll moment derivatives $C_{l\beta}$, C_{lp}, $C_{l\delta}$, rad^{-1}	−2.58, −15, 0.5901
Pitch moment derivatives C_{m0}, $C_{m\alpha}$, $C_{m\delta}$, C_{mq}, rad^{-1}	0.04, −5.73, −9.45, −105
Yaw moment derivatives $C_{n\beta}$, $C_{n\delta}$, C_{nr}, rad^{-1}	6.30, 7.54, −80
Pitch autopilot gains K_{1p}, K_{2p}, K_{3p}, K_{4p}	0.96, −0.09, −25.20, −1.72
Yaw autopilot gains K_{1y}, K_{2y}, K_{3y}, K_{4y}	1.34, 0.12, 31.55, 2.29
Roll autopilot gains $K_{1\phi}$, K_{1r}	18.31, 0.58
SFC, kg/(N · s)	0.0000406

dynamics and the angular accelerations, and these terms have been simplified in the model used for optimization.

The roll autopilot loop consists of an outer (angle) loop and an inner body-rate loop. With the inner body-rate loop, a body-rate demand is generated, and the achieved roll rate is fed back to augment the speed of response of the loop. A suitable approximation for the roll rate is thus

$$p_{\text{dem}} = K_{1\phi}(\phi_d - \phi) \tag{40}$$

$$p \approx p_{\text{dem}}/(1 + s\tau) \tag{41}$$

where $K_{1\phi}$ is the roll autopilot gain. The lag τ accounts for the dynamics of the roll rate response. A suitable value for the lag can be easily obtained from the roll loop transfer functions. Equations (40) and (41) are essentially a mapping from roll angle demand to roll rate that uses the autopilot transfer functions to obtain body rates. (A similar method can also be applied to the pitch and yaw autopilots.) The other simplification concerns the attitude dynamics, where cross-product terms due to roll rate in Eqs. (5) and (6) are neglected. Essentially, this means that the applied pitch and yaw moments alone generate pitch and yaw angular accelerations:

$$\dot{q} \approx M/I_{yy} \tag{42}$$

$$\dot{r} \approx N/I_{zz} \tag{43}$$

Further testing confirmed that very little fidelity is gained from including the cross-product terms, and so neglecting them is an acceptable approximation. Finally, we assume that the missile executes coordinated turns with small sideslip. This can be used to simplify the position differential equations because the y velocity component in body axes V in Eqs. (24–26) can be taken to be zero. After the optimal controls are computed, they are fed into the full six-DOF model in which the approximations explained in this section are removed. The differences between the two models are minor, thereby validating the model used for the optimal control calculations.

III. Optimal Control Problem Formulation

To compute the optimal controls, it is necessary to convert the main mission requirements into a mathematical optimal control problem. The key mission requirements include 1) minimizing the exposure time and peak height for stealth purposes; 2) minimizing the crossrange resolution during approach (ensuring high-resolution images are obtained); 3) ensuring satisfaction of mechanical and physical constraints, for example, gimbal angles and control bounds; 4) keeping the missile speed and incidence within satisfactory bounds; 5) lethality constraints (minimizing the miss distance and incidence at impact and satisfying and any impact angle constraint); and 6) ensuring adequate ground clearance.

A. Initial Conditions

The initial conditions of the missile are $R_{sx}(0) = 0$, $R_{sy}(0) = 0$, $R_{sz} = 60$, $U(0) = 272$, $V(0) = 0$, $W(0) = 0$, $\phi(0) = 0$, $\theta(0) = 0$, $\psi(0) = 0$, $p(0) = 0$, $q(0) = 0$, $r(0) = 0$, $m(0) = 1200$, $x_p(0) = 0$, $y_p(0) = 0$, and $T(0) = 4500$. These describe a missile with an initial mass of 1200 kg that is 60 m above sea level and is flying straight and level at Mach 0.8 using a nominal thrust of 4500 N.

B. Cost Function

The choice of cost function and constraint set for the missile control are described next. The following cost function was selected:

$$J = c_h \int_0^{t_f} \left[(R_{sz} - 30)^2 + \frac{c_t}{c_h} \right] \mathrm{d}t \tag{44}$$

which penalizes deviations away from the reference datum of 30 m, as well as the flight time. The scaling factors c_h and c_t ensure that these objectives are appropriately balanced. This choice of cost function is motivated by the need for a stealthy low-altitude approach. The c_t term is only used in the cases where variable throttle is considered. If the thrust is variable, the second term prevents the optimizer from reducing the turn radius by throttling off. Speed reductions of this type are undesirable because they lead to extended flight times and low impact speeds.

C. Control Bounds

The controls are bounded by the maximum allowable acceleration, as well as the maximum roll angle through which the airframe can be rotated. Thus,

$$|A_{zd}| \leq 40 \text{ ms}^{-2}, \qquad \forall t \in [0, t_f] \tag{45}$$

$$|\phi_d| \leq 80 \text{ deg}, \qquad \forall t \in [0, t_f] \tag{46}$$

which correspond to approximately 4-g pitch acceleration capability and 80 deg of bank angle. The acceleration capability impacts on the maximum turn rate of the missile and is particularly important in a radar imaging context because the missile may have to turn very rapidly to home-in on the target successfully. For controllable throttle scenarios, the bounds on the throttle setting are

$$0.2 \leq \epsilon \leq 1.0, \qquad \forall t \in [0, t_f] \tag{47}$$

where 1.0 corresponds to full demanded thrust and 0.2 is the lower bound on the throttle setting, corresponding to an idling mode for the engine. The control variables include the total pitch acceleration demand, the missile roll angle, and the throttle setting (when applicable).

D. Terminal Constraints

End position constraints, or target coordinates, are required and are based on estimates that the terminal guidance phase would start approximately 15 km away from the target. The crossrange offset is variable depending on the case studied. In the nominal case, it is assumed that no crossrange offset is imposed. The terminal position constraints are then

$$R_{sx}(t_f) = 15{,}000 \text{ m} \tag{48}$$

$$R_{sy}(t_f) = 0 \text{ m} \tag{49}$$

$$R_{sz}(t_f) = 20 \text{ m} \tag{50}$$

An aim-off point 20 m above the target is selected as the desired terminal z position. For a terminal impact angle of 15 deg from a vertical reference, a body attitude of −75 deg is needed. [The ideal

impact angle for lethality purposes is 0 deg from a vertical reference, corresponding to $\theta(t_f) = -90$ deg.] It is also desirable to minimize the incidence at the impact point to align the missile body and flight path so that the following constraints are imposed:

$$\theta(t_f) = -75 \text{ deg} \tag{51}$$

$$\alpha(t_f) = 0 \text{ deg} \tag{52}$$

E. Path Constraints

The path constraints arise from the need to respect a minimum ground clearance level, the seeker gimbal angle limits, speed constraints, and the DBS constraints. A state constraint that enforces a minimum ground clearance is

$$R_{sz} \geq 10 \text{ m}, \qquad \forall t \in [0, t_f] \tag{53}$$

This level is chosen arbitrarily and depends on the g capability of the missile, as well as its speed. It is important for the missile to steer clear of the transonic/supersonic region because the aerodynamics change rapidly near this region, making the missile airframe difficult to control. An upper speed limit is, therefore, imposed on the Mach number M_n:

$$M_n \leq 0.91, \qquad \forall t \in [0, t_f] \tag{54}$$

which corresponds to an upper speed limit of 310 ms^{-1} at sea level. For a gimbaled seeker, the gimbal angle limits are an important consideration. For an inner pitch, outer roll gimbaled seeker, a pitch gimbal angle limit of 45 deg is imposed:

$$|\Theta| \leq 45 \text{ deg}, \qquad \forall t \in [0, t_f] \tag{55}$$

The roll gimbal is not constrained by any mechanical angle limits. The requirement for radar imaging is more difficult to handle because it is not obvious how to guarantee a desired crossrange resolution at any specified range. One method is to specify the desired crossrange resolution as a function of range and impose a path constraint. The DBS angles and speed will then be determined implicitly [through Eq. (39)] to satisfy the imaging requirements. However, the crossrange resolution function in Eq. (39) is not well-behaved numerically, and singularities exist at zero DBS azimuth angle ($\Xi = 0.0$). For a nominal missile speed and fixed seeker parameters, the main factor impacting on the crossrange resolution is the azimuth angle between the velocity and the sightline. Up to handover to real-beam guidance, that is, up to approximately 2-km range to go, the azimuth angle should be maintained between 10 and 40 deg, the upper limit being constrained by the gimbal angle limits and the maximum g capability of the missile. The exact angle required depends on the crossrange resolution desired and the integration period δt in Eq. (39). It is clear that if larger DBS azimuth angles are developed, more control action near the end of the trajectory will be required to intercept the target. Following handover, the DBS azimuth angle will decrease, possibly rapidly, to zero to home in on the target. To assist the optimization process, the azimuth angle is controlled using a smooth function. A path constraint is then imposed on the DBS azimuth angle using this function. The form of the function is obtained by adding exponential and cosine functions that are parameterized by the downrange:

$$f(R_{sx}) = d_0 + \cos^2[d_1(R_{sx} + d_2)] + d_3 \exp[d_4(R_{sx} - d_5)] \tag{56}$$

where the coefficients d_i are appropriately chosen constants. The coefficients for the nominal case (case A) were selected so that the profiling function matches the broad characteristics of the DBS azimuth angle in previous studies; see Refs. 4 and 22. Manual tuning of the coefficients was performed for the other cases to obtain an appropriate angle behavior. Although the downrange is used in this example, it is possible to use the range or time to go instead. The constant d_0 is a small constant that acts as an offset. This term prevents the use of large actuation signals near the initial time. The cosine squared term controls the rolloff of the DBS azimuth angle, and d_1 ensures that an appropriate segment of the cosine squared function is elongated over the 0–15 km downrange axis. The exponential term ensures that the DBS azimuth angle can reduce to zero, which allows the missile to intercept the target. The cosine of the DBS azimuth angle is then required to be less than this function over the whole trajectory, that is,

$$\cos(\Xi) \leq f, \qquad \forall t \in [0, t_f] \tag{57}$$

The use of $\cos(\Xi)$ ensures that it does not matter whether the missile is at a negative or positive crossrange with respect to the target because a cosine function is an even function. Other types of behavior can be parameterized by using the function in Eq. (56). Because the paper investigates different initial geometries, different functions are used for each test case. The coefficients used are listed in Table 3. Case C permits the use of DBS up to a short (approximately 500-m) range to go, whereas the other cases require the seeker to switch out of DBS mode at approximately 2-km range to go. An example of the typical angle behaviors required for each test case can be obtained by inserting the constants for each test case into Eq. (56). The angle profiles used for each test case are displayed in Fig. 3 as a function of downrange. Although these functions specify the desired angle behavior, the exact DBS angle obtained may deviate from the boundary of these functions [though still satisfying Eq. (57)]. This is dependent on the weighting on the DBS constraint and the relative weightings of the cost function and the other constraints. (See Sec. III.G, for further details.)

Table 3 Constants for profiling functions

Case	Constants
A	$d_0 = 0.0068$, $d_1 = 0.000024$, $d_2 = 1000$, $d_3 = 0.0152$, $d_4 = 0.00067$, $d_5 = 11{,}400$
B	$d_0 = -0.0170$, $d_1 = 0.00001$, $d_2 = 1000$, $d_3 = 0.0090$, $d_4 = 0.00072$, $d_5 = 12{,}500$
C	$d_0 = 0.004$, $d_1 = 0.000025$, $d_2 = 1000$, $d_3 = 0.0118$, $d_4 = 0.00077$, $d_5 = 11{,}700$

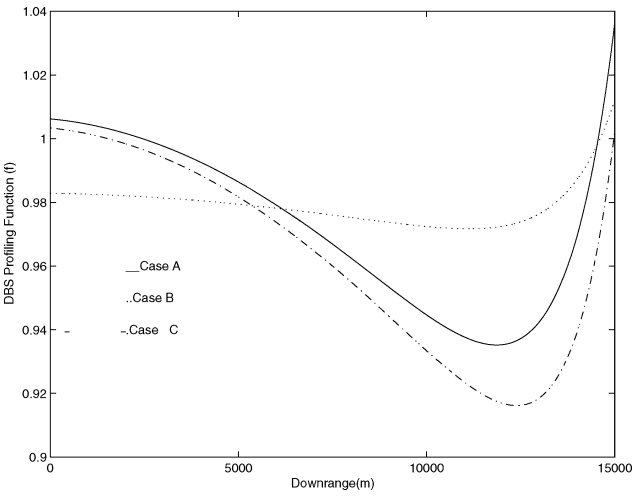

Fig. 3 Profiling functions for DBS angle behavior.

F. Choice of Initial Controls and Final Time

It is necessary to supply the optimization algorithm with initial estimates for the control variables (pitch acceleration and roll demand) and the final time. The scenarios considered in this paper differ in the amount of crossrange offset, and so the initial controls and final time are different for each case. The functional form of the initial controls can be represented as polynomial functions of time:

$$A_{zd}(0) = p_4 t^4 + p_3 t^3 + p_2 t^2 + p_1 t + p_0 \tag{58}$$

$$\phi_d(0) = r_2 t^2 + r_1 t + r_0 \tag{59}$$

where $A_{zd}(0)$ and $\phi_d(0)$ refer to the control variables before running the optimization algorithm (iteration 0). The values for the

Table 4 Initial estimates for final time and controls

Offset	$t_f(0)$	Roll coefficients	Pitch coefficients
3 km	56.5	$r_0 = 0.44$, $r_1 = -0.02$, $r_2 = 2.09 \times 10^{-4}$	$p_0 = -11.17$, $p_1 = 0.15$, $p_2 = -0.007$, $p_3 = 1.32 \times 10^{-4}$, $p_4 = -9.25 \times 10^{-7}$
0 and 1 km	54.0	$r_0 = 0.0$, $r_1 = 0.0$, $r_2 = 0.0$	$p_0 = -9.81$, $p_1 = 0.0$, $p_2 = 0.0$, $p_3 = 0.0$, $p_4 = 0.0$

Table 5 Scaling factors

Constraint	Scaling factor
Cost function c_h	10^{-7}
Cost function c_t	0.04
Terminal position constraints	0.01
Terminal pitch angle constraint	10.0
Terminal incidence constraint	10.0
DBS imaging constraint	1000
Mach constraint	10.0
Ground clearance constraint	0.1
Gimbal angle constraint	100

coefficients, along with the final time estimate, are shown in Table 4. Note that for the 0- and 1-km offset cases the same initial estimate is used. The final time estimates in these cases were obtained by dividing the terminal downrange ordinate by an average speed estimate. In the 3-km offset case, a conventional closed-loop guidance method (proportional navigation in the horizontal plane and height control in the vertical plane) was used to obtain the initial estimate. If the throttle is a control variable, these estimates are supplemented with

$$\epsilon(0) = 1.0 \tag{60}$$

These continuous control functions are then converted into discretized initial estimates by the procedure described in Sec. III.H.

G. Scaling Factors For Problem

The objective function and the associated constraints have to be scaled to ensure that the various tradeoffs are properly weighted against each other. It is advisable that the constraints and cost function have the same order of magnitude. Larger weights on the path constraints were found to be more effective in avoiding large transgressions and improving convergence. Table 5 lists the constraints and the scaling factors used here. The cost function weightings correspond to the c_h and c_t factors introduced in Eq. (44), where c_t is set to zero if full throttle is assumed.

H. Optimization Parameters

Numerical methods for solving optimal control problems have advanced significantly over the past decade, and a good overview can be found in Ref. 25. The various approaches are characterized as direct and indirect methods. Indirect methods use the necessary conditions of optimality (the minimum principle) to convert the optimal control problem into a two-point boundary value problem that can be solved numerically using shooting methods. Direct methods solve the optimization problem via a discretization scheme in conjunction with nonlinear programming. The states and controls may be nonlinear programming variables (full discretization), in which case equality constraints relating to the state equations are imposed. The resulting nonlinear programming problem can be solved efficiently using large-scale quadratic programming methods that exploit sparsity.[25] Alternatively, a smaller-sized problem is obtained if the state trajectories are determined recursively using a suitable integration algorithm, and the control space is searched for solutions (control discretization). The algorithm employed in this study uses piecewise constant functions to parameterize the control functions and a Radau IIA integration algorithm to integrate the state equations. Adjoint variables are introduced to calculate the gradients. An exact penalty function is used to deal with constraints, and the Hessian is approximated using quasi-Newton updates. More details on the algorithm design, the convergence analysis, and the performance for sample optimal control problems are contained in Ref. 3.

Table 6 Optimization parameters

Optimization parameter	Value
Optimality tolerance	10^{-5}
Number of discretization intervals N	400
Relative tolerance for state equations	10^{-3}
Absolute tolerance for state equations	10^{-3}

Each control variable is discretized into a grid of $N-1$ intervals, and the piecewise constant values are adjusted on each iteration. The continuous controls are, thus, discretized and parameterized as follows:

$$A_{zd}(t) = \sum_{i=1}^{N} p_i(t) A_{zd}(i), \qquad \forall t \in [0, t_f] \tag{61}$$

$$\phi_d(t) = \sum_{i=1}^{N} p_i(t) \phi_d(i), \qquad \forall t \in [0, t_f] \tag{62}$$

$$t_i = i t_f / N, \qquad i = 1, 2, \ldots, N \tag{63}$$

$$p_i(t) = 1.0, t \in [t_i, t_{i+1}] \tag{64}$$

$$p_i(t) = 0.0, t \notin [t_i, t_{i+1}] \tag{65}$$

Clearly, the optimization vector to be determined is composed of $A_{zd}(i)$ and $\phi_d(i)$, and the cost function and constraints can be replaced by their discretized equivalent forms. Note that both $A_{zd}(i)$ and $\phi_d(i)$ can take on any value within their bounds, and the final time t_f is also an optimization variable. The nonlinear programming variables are adjusted on each major iteration to shape the trajectory. The optimization parameters used are listed in Table 6. If a more accurate solution is required, the integration tolerances can be reduced, resulting in a finer mesh. For the cases with controllable throttle, a similar discretization scheme is applied to the throttle setting, and the number of optimization parameters is increased by N.

IV. Results

The aim of this section is to present and analyze three case studies. In each case, an initial downrange offset of 15 km is assumed. By varying the initial crossrange offset and impact angle constraints it is possible to examine how the optimal controls and trajectories would vary for these different mission profiles. The results of cases A and B assume a switch to real-beam guidance at 2-km range to go, and the DBS azimuth angle is usually reducing by this range to go. In contrast, case C examines the feasibility of using DBS up to a much shorter range to go (500 m) with a reduced terminal pitch impact angle (45 deg). The differences between the cases are summarized in Table 7. A number of performance metrics are included for each case, enabling a comparison to be undertaken: 1) The missile exposure time is calculated as the time spent above 100-m altitude. 2) The bunt range is defined as the range to go when the missile crosses the 100-m exposure height for the first time. All of the test cases represent converged solutions to the optimization problem, and all constraints are satisfied according to the optimality tolerance (adjusted by any scaling factors). For instance, the terminal position accuracy will be of the order of 10^{-3} m and both the incidence at

Table 7 Summary of cases

Constraint/control variables	Case A	Case B	Case C
Terminal crossrange offset, km	0.0	3.0	1.0
Thrust controllable	No	Yes	No
Number of control variables	2	3	2
Terminal pitch angle, deg	−75	Free	−45
Terminal yaw angle, deg	Free	Free	−86

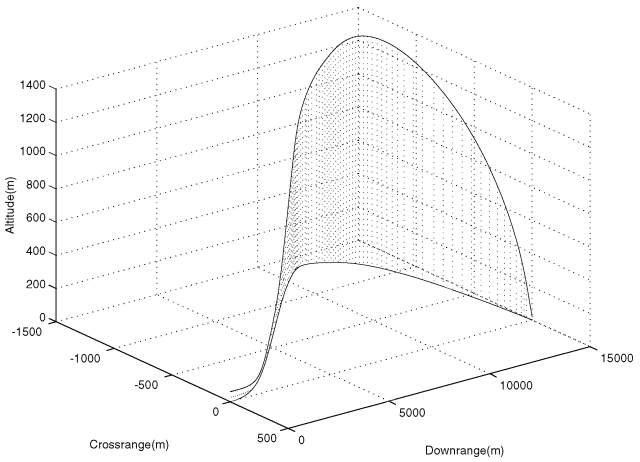

Fig. 4 Three-dimensional trajectory (case A).

impact and impact angle error will be satisfied to a similar degree of accuracy.

A. Case A: 0-Kilometer Offset

In the first case, it is assumed that the missile has no initial crossrange offset. To obtain the DBS azimuth angle, it is necessary to develop a crossrange offset so that the missile has to fly away from the target initially in the ground plane to develop the necessary crossrange offset for imaging purposes. This type of behavior can be found in Ref. 22, where a similar ground plane trajectory is generated for a STT missile. The maximum crossrange offset required will depend on how large the DBS azimuth angle is required to be, which is principally determined by the profiling function constraint in Eq. (56). The trajectories and controls are shown in three dimensions in Fig. 4, with the two-dimensional plots shown in Figs. 5 and 6. In Figs. 5 and 6, the outputs of the six-DOF model with the approximations of Sec. II.F removed are displayed as well (dotted lines). Because the six-DOF position outputs match the optimal position states very well, the dotted lines in Figs. 5 and 6 are barely discernible. The deviations are an approximately 13-m difference in peak height and a 3-m difference in the maximum crossrange offset, thereby validating the model used for optimal control calculations.

As can be seen from Fig. 6, the missile initially uses 50 deg of negative roll angle to steer away from the target and develop a crossrange offset. After an appropriate heading angle is achieved, the missile maintains this heading angle (by maintaining a small roll angle) up to approximately 10.5 km downrange. The missile then gradually increases its roll angle to turn back toward the target. Increasing amounts of roll angle are used up until 12 km downrange when the roll angle hits its saturation limit of 80 deg. When the pitch command changes sign (from negative to positive in Fig. 5), negative roll angle is needed to turn the missile toward the target over the last 2–3 km in downrange. This is because the lift vector is pointing downward after 12.5 km downrange. In contrast, at longer ranges, for example, 1 km downrange, where the lift vector is pointing upward, a positive roll angle will turn the missile toward the target. This "snap roll" is a feature of BTT trajectories[11] and is more pronounced with more aggressive trajectories. The snap roll couples into the seeker dynamics and is also dependent on the roll angle control bounds. The snap roll in this example occurs at approximately 12.5 km. At

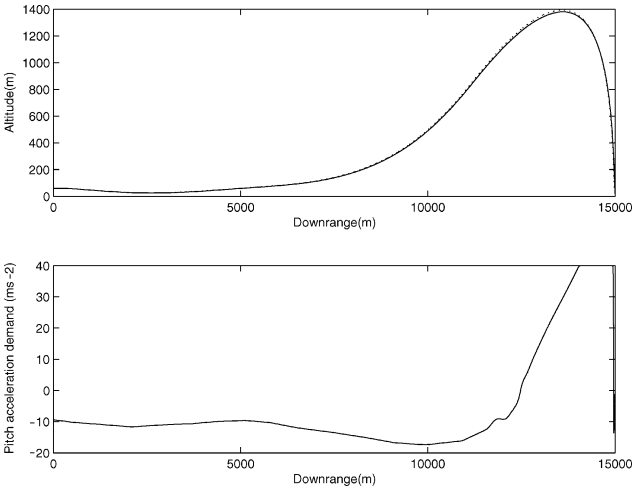

Fig. 5 Downrange/altitude profile and control (case A).

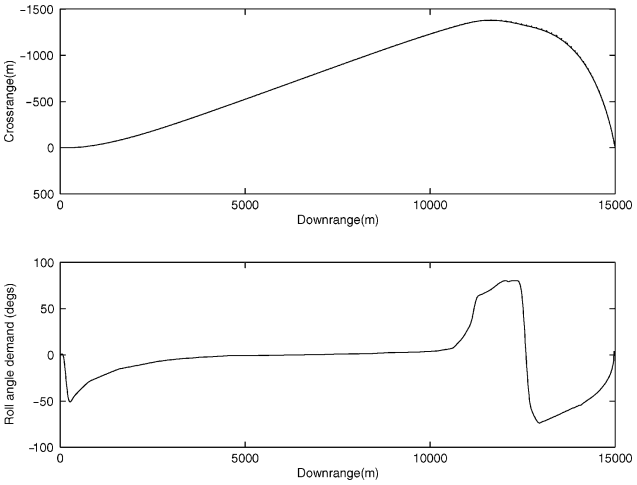

Fig. 6 Downrange/crossrange profile and control (case A).

13 km downrange, the DBS azimuth angle has to be maintained, and so the missile tends to offset its velocity vector from the target sightline vector, resulting in a curved approach toward the target. The roll angle does not reach its negative saturation limit after the snap-roll because the magnitude of the pitch control facilitates the generation of sideforce and the DBS azimuth angle is permitted to reduce after 2-km range to go. The roll angle is then driven back to zero over the final 2 km of downrange as the missile rolls back to a wings level orientation in roll. The missile's velocity vector becomes aligned with the target sightline (at approximately 500-m range to go), and the missile impacts the target with the specified impact angle. The DBS azimuth angle and crossrange resolution are shown in Fig. 7 as a function of downrange. The x axis in Fig. 7 is truncated near the 14-km limit (at approximately 2-km range to go) because the crossrange resolution becomes infinitely large when the DBS azimuth angle Ξ approaches zero. The initial crossrange resolution is also poor because the DBS azimuth angle is initially zero, and so the first 10 s (approximately 3 km downrange) is truncated so that Fig. 7 is appropriately scaled.

The crossrange resolution is excellent in the critical 11–14-km downrange interval (corresponding to approximately 4–2-km range to go). A minimum crossrange resolution of less than 0.5 m is achieved for all DBS integration periods. The sideslip angle is kept small (less than 0.5 deg) throughout the trajectory. Periods of peak roll rate tend to occur near the bank reversal time and near the end of the trajectory, but these effects do not induce control surface saturation.

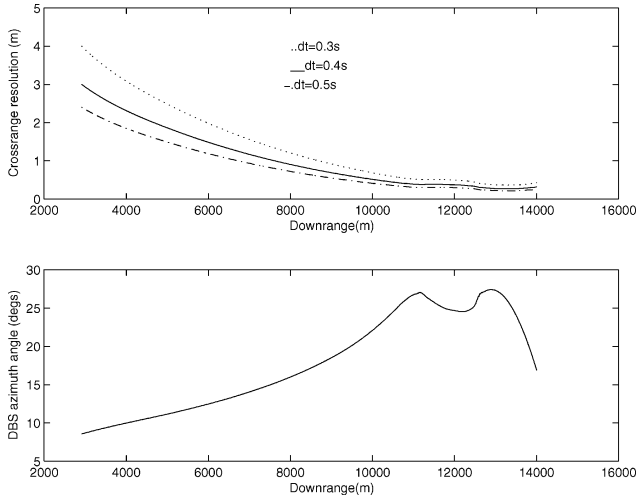

Fig. 7 DBS azimuth angle and crossrange resolution (case A).

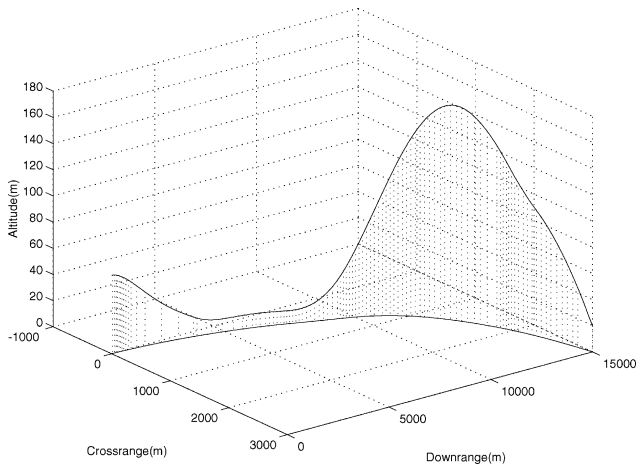

Fig. 8 Three-dimensional trajectory (case B).

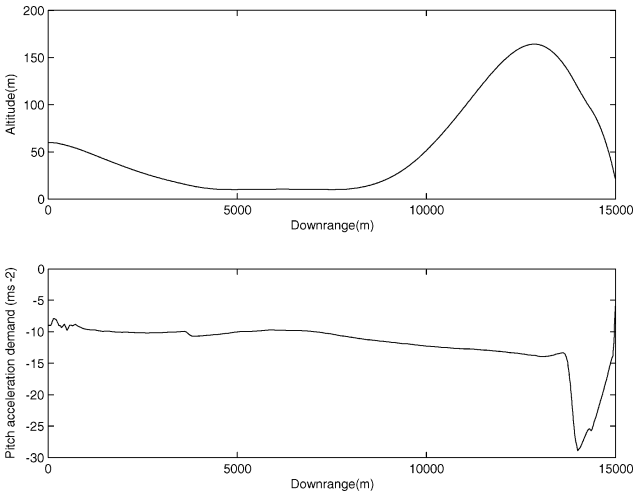

Fig. 9 Downrange/altitude profile and control (case B).

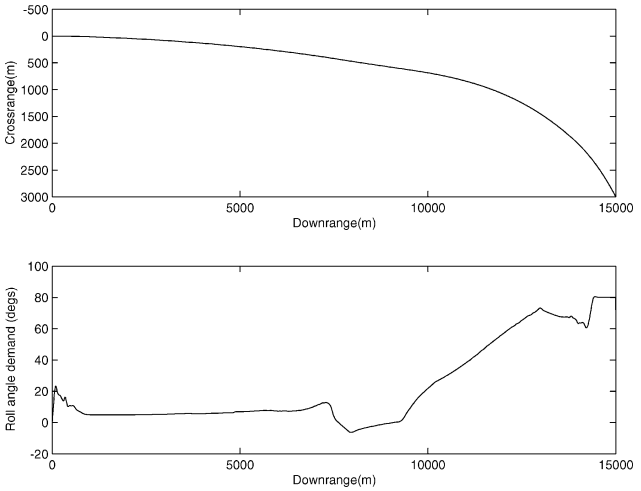

Fig. 10 Downrange/crossrange profile and control (case B).

B. Case B: 3-Kilometer Offset with No Impact Angle Constraint

The next case relaxes the need for a bunt trajectory because a free terminal impact angle is specified. Because the upper Mach constraint may now become active in this scenario, the throttle is set as a control variable. In this case, the applied thrust is modulated by the throttle setting, which allows us to examine whether the full thrust assumption is really justified from an optimality point of view. The position states and the pitch and roll controls are shown in Figs. 8, 9, and 10, respectively.

In contrast to the preceding case, both the pitch and roll control are unidirectional, which eliminates the snap-roll feature evident in case A. One unexpected feature of the missile trajectory was a slight bunt maneuver that requires a maximum height of approximately 164 m. Also, the missile drops to its minimum altitude constraint before the "mini-bunt." This mini-bunt feature is due to the coupling of the roll and pitch controls in a BTT system. To turn quickly near the end of the trajectory in the ground plane, the missile needs a larger pitch command that converts lift into sideforce via a large roll angle. This is accomplished by climbing gradually and then invoking approximately 3.0 g of pitch demand after the apogee. This feature is consistent with the expectation that with BTT a small turn radius (associated with a steeper bank angle) is accompanied by a loss of altitude. It is also evident that, in comparison with the preceding case, to flip the missile at the apogee requires less sustained pitch demand because the maximum height and maximum flight-path angle are also reduced. By examination of the controls as the roll control nears its 80-deg saturation limit, most of the lift generated by the 3.0-g peak pitch demand is converted to sideforce, and the missile uses a combination of gravity and the small vertical component of lift to turn in the vertical plane. This was confirmed by transforming the applied acceleration into inertial axes and comparing the z component of acceleration with the magnitude of the acceleration due to gravity. The bunt maneuver could be suppressed by imposing a maximum height constraint, but this would compromise the DBS requirements.

Another important feature of this case is that the Mach constraint becomes active before and during the climb because the climb is at a relatively shallow flight-path angle (less than 3 deg). The throttle is regulated to keep the missile's speed up against the Mach boundary. The missile also hits the target with an impact speed of Mach 0.91, which is an improvement over the preceding case. This tight control of the throttle setting (coordinated with the other two controls) is a desirable property and is an indication that the optimization algorithms are working properly. The throttle setting and Mach number are displayed in Fig. 11 and the DBS azimuth angle and crossrange resolution in Fig. 12. Note that the incidence angle increases sharply with the 3.0-g pitch demand, resulting in increased drag during the descent. The increase in drag is offset by a return to full throttle at approximately 14 km downrange. Because the missile starts to gain speed during the descent (under gravity), it is necessary to reduce the throttle to stay on the Mach boundary. This is clearly evident in Fig. 11 toward the end of the mission.

In comparison with case A, the total flight time is reduced by 5 s due to a combination of the free impact angle and the controllable throttle. Although the DBS azimuth angle is reduced compared with case A, the crossrange resolution obtained is similar to case A. This is through the higher speed V_t and lower DBS elevation angle Λ associated with the relaxed bunt.

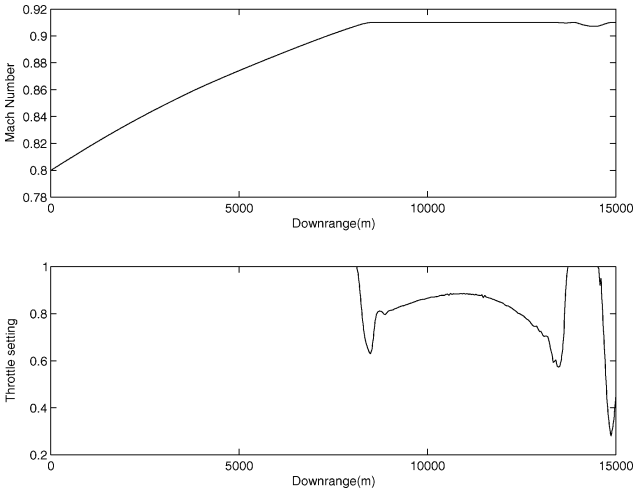

Fig. 11 Mach number and throttle setting (case B).

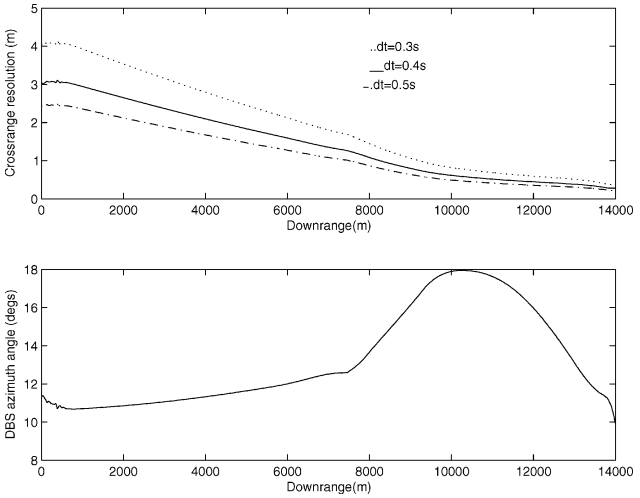

Fig. 12 DBS azimuth angle and crossrange resolution (case B).

C. Case C: 1-Kilometer Offset with Terminal Azimuth Angle and DBS Short-Range Guidance

In the final example, a 1-km initial crossrange offset is imposed with a steep terminal yaw angle constraint (Table 7). The terminal yaw angle constraint forces the missile to overshoot the target in crossrange before homing in along the desired approach direction, that is, the missile must approach the target from its back. A further significant difference over preceding cases studied is that we require DBS to be used up to a much shorter range (approximately 500 m). This is of interest because the requirements for the seeker tracking and aimpoint optimization algorithms are eased if DBS can be used up until the reduced range. The states and controls are shown in Figs. 13–15.

The position plots in Fig. 15 show that after the missile reaches its maximum crossrange offset (2.8 km), at 11 km downrange, the flight path moves gradually back toward the target to maintain the DBS azimuth angle up until a short range. This behavior is a direct consequence of the short-range DBS requirement. The roll control has a large initial transient that enforces a large change in heading. A positive roll angle is then used over the first 6 km in downrange to increase the missile position in crossrange. This is followed by a gradual decrease in roll angle to approximately -45 deg of roll angle that enforces the turn back toward the target. As with case A, a snap roll is evident in the roll angle profile, though it is rather more gradual and is negative to positive as a consequence of the engagement geometry. In the terminal homing phase (13–15 km downrange) the roll angle is close to saturation, but comes off of its saturation boundary near the end of the flight. This reduction in the roll angle is due to the impact angle constraint, which requires the use of more lift. The DBS azimuth angle and crossrange resolution are displayed in Fig. 16, where the downrange axis is extended to correspond to a 500-m range to go. Note that in Fig. 16 the DBS azimuth angle passes through zero early in the trajectory, and so the first 2 km in downrange is truncated to highlight the main features of Fig. 16.

With the crossrange resolution expression [Eq. (39)] there are two terms that are of importance at short ranges. The crossrange resolution decreases linearly with range and inversely with the sine

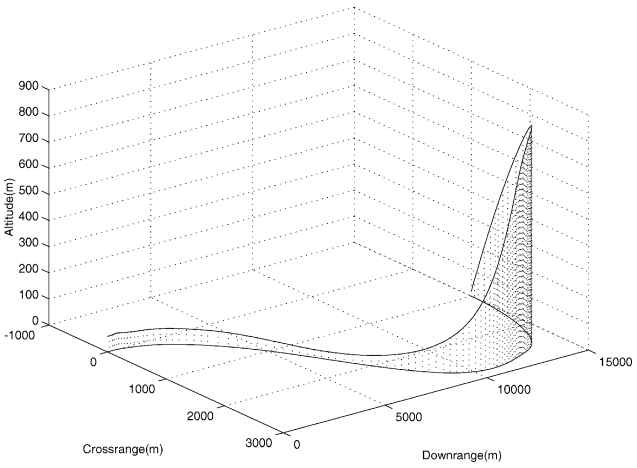

Fig. 13 Three-dimensional trajectory (case C).

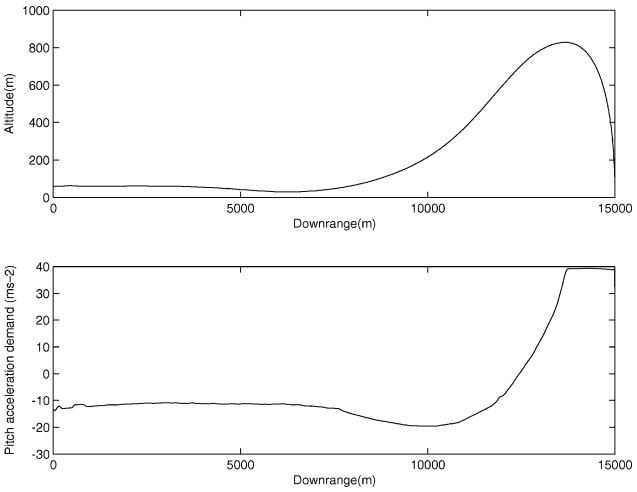

Fig. 14 Downrange/altitude profile and control (case C).

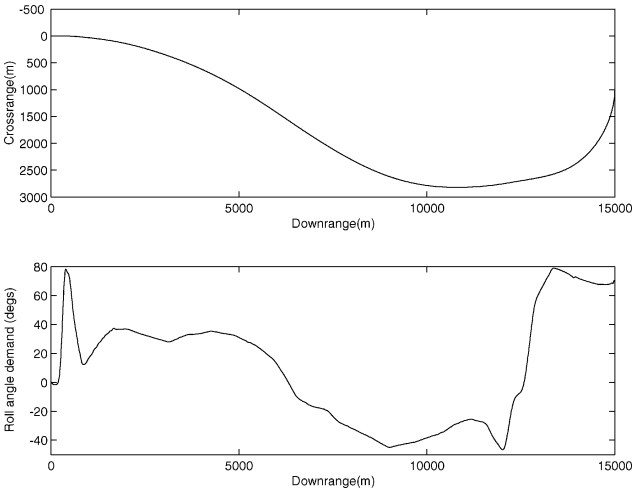

Fig. 15 Downrange/crossrange profile and control (case C).

Table 8 Performance summary for test cases

Performance measures	Case A	Case B	Case C
Max. height, m	1380	164	829
Final time, s	57.410	52.330	57.315
Exposure time, s	33.91	14.91	25.6
Max. incidence, deg	11.39	3.81	9.71
Max. sideslip, deg	0.45	0.12	0.40
Resolution at 2 km, m	0.41, 0.31, 0.25	0.45, 0.34, 0.27	0.22, 0.17, 0.13
Resolution at 500 m, m	——	——	0.22, 0.16, 0.13
Minimum resolution, m	0.36, 0.27, 0.22	0.37, 0.28, 0.22	0.21, 0.15, 0.12
Impact speed, ms^{-1}	268	309.6	267.8
Min speed, ms^{-1}	256	272	265.2
Max. climb angle, deg	19.09	2.85	13.03
Bunt range, km	8.32	4.50	6.48
Max. roll rate, deg/s	182	120	172
Final cost	2.3755	2.1099[a]	0.69857
Max. crossrange offset, m	1379	3000	1819
Heading impact angle, deg	64.1	52.97	−86.0
Flight-path impact angle, deg	−75	−5.81	−45
Max. pitch gimbal angle, deg	44.50	18.26	39.79

[a]Cost function includes flight time penalty.

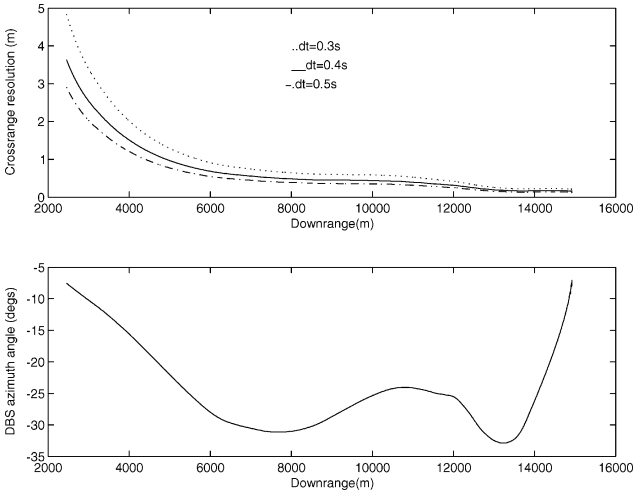

Fig. 16 DBS azimuth angle and crossrange resolution (case C).

of the DBS azimuth angle Ξ, and so there may be some degradation in resolution if Ξ approaches zero while the range R is large. In this example, Ξ is large enough such that there is no degradation in the crossrange resolution up to very short ranges (less than 300 m), and the crossrange resolution stays approximately constant over the 2-km–500-m range-to-go period. This is because the DBS azimuth angle reduction is offset by the range reduction. Much improved DBS imaging performance is observed compared with the preceding cases (between a 0.1- and 0.2-m improvement in crossrange resolution at 2 km compared with case A), and, unlike the other cases, this trajectory permits the use of DBS up to 500-m range to go with the same DBS integration period. Compared with the other cases, the trajectory is also quite favorable in terms of the control action, the maximum height, and the exposure time. The more aggressive groundplane trajectory does influence the impact angle because a maximum height of 830 m is required for a relatively modest impact angle (−45 deg). This suggests that for more aggressive DBS trajectories, for example, trajectories requiring DBS guidance to short ranges, the impact angle requirements should be relaxed, otherwise the bunt range and exposure time will increase significantly. The imposition of a terminal yaw angle constraint seems to have benefits for DBS guidance because it increases the trajectory's curvature and the maximum crossrange offset. These both influence the maximum angular offset developed.

D. Comparison of Cases

The performance in the three case studies is summarized in Table 8. Note that for case C the crossrange resolution at 500 m is stated (rather than 2 km for the other cases) because this is the more relevant benchmark for this example. The maximum crossrange offset is referenced to the target position in the y direction rather than the initial missile crossrange. The asterisk in Table 8 indicates the use of the modified cost function in which the flight time penalty was included. In terms of imaging, the trajectories for cases A and B are quite similar in terms of the crossrange resolution obtained. With case C the use of DBS up until short ranges results in much improved imaging performance with less than 0.25-m crossrange resolution obtained for all DBS integration periods. The speed profiles for cases A and C are quite similar (owing to the full thrust assumption). The exception is case B, where the mini-bunt results in a modest climb angle and the thrust is regulated to stay on the upper Mach boundary throughout the bunt maneuver. The maximum sideslip observed is less than 2 deg for each case, which is consistent with the coordinated steering assumption. Larger roll rates and fin angle deflections tend to occur at the start and end of the trajectory, as well as at the snap roll, but otherwise these variables are kept quite small throughout the trajectory. This is important for the space stabilization of the seeker and the maintenance of sufficient control surface authority with which to reject disturbances.

Apart from the imaging performance, the other aspect of the trajectories that are of interest are the missile exposure time, the bunt range, and the maximum height. The results suggest that bunt ranges of between 6 and 8 km are required for impact angles of between 15 and 45 deg. However, this is dependent on the type of DBS trajectory flown. For case C the impact angle would be improved (for the same maximum height) if a less aggressive DBS trajectory were flown. The results suggest that missile exposure times are likely to be between 20 and 35 s, depending on the impact angle constraint. For this particular airframe, the maximum incidence required is approximately 11 deg for case A, which has the steepest terminal flight-path angle (−75 deg). Although not stated in Table 8, the miss distance and incidence at impact are very small, because these are hard constraints in the optimization process.

V. Conclusions

A methodology for computing optimal terminal guidance trajectories for air-to-surface guided missiles with radar imaging seekers is presented. This guidance problem is demanding because the optimal trajectories have to satisfy terminal constraints for lethality purposes as well as path constraints that are dictated by the missile dynamics and the radar imaging system. The optimal trajectories are characterized by a bunt maneuver, which is used to satisfy terminal angle constraints as well as to minimize the missile's exposure to air-defense units. In addition, a crossrange offset may have to be developed to achieve adequate crossrange resolution from the radar imaging system. The missile airframe considered requires the use of

BTT steering, which introduces some interesting tradeoffs because the two controls are strongly coupled.

The guidance problem can be elegantly solved by recasting it as an optimal control problem that can be solved using numerical optimization. This solution framework allows the tradeoffs between competing constraints to be examined, and it provides insight into the nature of the optimal controls derived. The feasibility of using DBS up to short ranges is also investigated. The results suggest that the optimizer is able to resolve the various tradeoffs very effectively.

It is demonstrated that a bunt maneuver is beneficial for DBS trajectories with BTT steering because the missile can use the increased pitch commands associated with a bunt maneuver to decrease the radius of turn in the groundplane. This benefit is offset by the reduced rate at which the missile can turn in the vertical plane, implying that larger altitudes and longer exposure times may be needed for an impact angle constrained flight plan. For DBS usage up to low range to go distances, the missile has to make a tight terminal-phase turn in its groundplane trajectory with the limit being set by gimbal angle limits and the airframe maneuverability.

Extensions to this work concern the development of closed-loop guidance laws for DBS imaging. The optimal trajectories generated in this study can be used as references for a trajectory tracking controller. There are a variety of approaches to the closed-loop implementation problem, and optimal preview control is one promising method currently being studied.

Appendix: DBS Angle Calculations

In this Appendix, the angles between the velocity vector and sightline in azimuth and elevation are briefly derived. First, we define a sightline vector that can be obtained from the missile/target relative geometry:

$$x_o = R_{sx}(t) - R_{sx}(t_f) \tag{A1}$$

$$y_o = R_{sy}(t) - R_{sy}(t_f) \tag{A2}$$

$$z_o = R_{sz}(t_f) - R_{sz}(t) \tag{A3}$$

It is convenient to normalize these by the range; hence,

$$x_s = x_o \Big/ \sqrt{x_o^2 + y_o^2 + z_o^2} \tag{A4}$$

$$y_s = y_o \Big/ \sqrt{x_o^2 + y_o^2 + z_o^2} \tag{A5}$$

$$z_s = z_o \Big/ \sqrt{x_o^2 + y_o^2 + z_o^2} \tag{A6}$$

These components define a unit sightline vector of unit length. The unit velocity vector in inertial axes is defined as

$$V'_{sx} = V_{sx} \Big/ \sqrt{V_{sx}^2 + V_{sy}^2 + V_{sz}^2} \tag{A7}$$

$$V'_{sy} = V_{sy} \Big/ \sqrt{V_{sx}^2 + V_{sy}^2 + V_{sz}^2} \tag{A8}$$

$$V'_{sz} = V_{sz} \Big/ \sqrt{V_{sx}^2 + V_{sy}^2 + V_{sz}^2} \tag{A9}$$

Because the unit velocity vector and unit sightline vector are expressed in a common frame, the total angle between the two vectors can be calculated by using a vector dot product. Because the vectors are of unit length, then

$$\Theta_T = \cos^{-1}(V'_{sx}x_s + V'_{sy}y_s + V'_{sz}z_s) \tag{A10}$$

This is the total angle between the velocity vector and the sightline. To calculate the individual azimuth and elevation angles, the unit sightline vector is first rotated into velocity axes. In component form,

$$x_{sw} = \cos(\gamma)\cos(\chi)x_s + \cos(\gamma)\sin(\chi)y_s - \sin(\gamma)z_s \tag{A11}$$

$$y_{sw} = -\sin(\chi)x_s + \cos(\chi)y_s \tag{A12}$$

$$z_{sw} = \sin(\gamma)\cos(\chi)x_s + \sin(\gamma)\sin(\chi)y_s + \cos(\gamma)z_s \tag{A13}$$

The azimuth and elevation DBS angles can then be calculated from

$$\Lambda = \tan^{-1}\left(z_{sw} \Big/ \sqrt{x_{sw}^2 + y_{sw}^2}\right) \tag{A14}$$

$$\Xi = \tan^{-1}(y_{sw}/x_{sw}) \tag{A15}$$

and it can be verified that

$$\cos(\Theta_T) = \cos(\Lambda)\cos(\Xi) \tag{A16}$$

This completes the proof.

Acknowledgment

The results presented in this paper were supported by funding from MBDA UK, Ltd.

References

[1]Edde, B., *Radar: Principles, Technology, Applications*, Prentice–Hall, Upper Saddle River, NJ, 1993, pp. 616–627.

[2]Stimson, G. W., *Introduction to Airborne Radar*, 2nd ed., SciTech, Mendham, NJ, 1998, pp. 393–437.

[3]Pytlak, R., *Numerical Methods for Optimal Control Problems with State Constraints*, Lecture Notes in Mathematics, Vol. 1707, Springer-Verlag, Berlin, 1999.

[4]Farooq, A., and Limebeer, D. J. N., "Trajectory Optimization for Air-to-Surface Missiles with Imaging Radars," *Journal of Guidance, Control, and Dynamics*, Vol. 25, No. 5, 2002, pp. 876–888.

[5]Kaufmann, W. A., "Flight Control Design Issues in Bank-to-Turn Missiles," *AGARD Lecture Series 173: Missile Interceptor Guidance System Technology*, AGARD, 1990, pp. 3-1, 3-16.

[6]Lin, C., Cloutier, J. R., and Evers, J. H., "High Performance Robust Bank-to-Turn Missile Autopilot Design," *Journal of Guidance, Control, and Dynamics*, Vol. 18, No. 1, 1995, pp. 46–53.

[7]Arrow, A., and Williams, D. E., "Comparison of Classical and Modern Missile Autopilot Design and Analysis Techniques," *Journal of Guidance, Control, and Dynamics*, Vol. 12, No. 2, 1989, pp. 220–227.

[8]Wise, K. A., "Bank-to-Turn Missile Autopilot Design Using Loop Transfer Recovery," *Journal of Guidance, Control, and Dynamics*, Vol. 13, No. 1, 1990, pp. 145–152.

[9]No, T. S., Cochran, J. E., and Kim, E. G., "Bank-to-Turn Guidance Law Using Lyapunov Function and Nonzero Effort Miss," *Journal of Guidance, Control, and Dynamics*, Vol. 24, No. 2, 2001, pp. 255–260.

[10]Cliff, E. M., Bocvaro, S., and Lutze, F. H., "Hierarchical Modeling Approach In Aircraft Trajectory Optimization," *Proceedings of the IFAC Automatic Control in Aerospace Conference*, International Federation of Automatic Control, Laxenburg, Austria, 1994, pp. 17–22.

[11]Pierson, B. L., Ong, S. Y., and Lin, C.-F., "2-D and 3-D Minimum Time to Turn Flights by Parameter Optimization," *Proceedings of the IEEE Regional Conference on Aerospace Control Systems*, Inst. of Electrical and Electronics Engineers, Piscataway, NJ, 1993, pp. 469–474.

[12]Dabney, J. B., and Miele, A.,"Variable Load Factor Guidance for Low-Altitude Fly-to-Point Maneuvers of a Jet Fighter Aircraft," *Journal of Dynamical and Control Systems*, Vol. 10, No. 2, 2000, pp. 195–212.

[13]Bryson, A. E., and Jardin, M. R., "Neighboring Optimal Aircraft Guidance in Winds," *Journal of Guidance, Control, and Dynamics*, Vol. 24, No. 4, 2001, pp. 710–715.

[14]Roenneke, A. J., and Well, K. H., "Linear Optimal Control for Re-entry Flight," *Computational Optimal Control*, International Series of Numerical Mathematics, edited by R. Bulirsch and D. Kraft, Birkhaeuser Verlag, Berlin, 1994, pp. 339–348.

[15]Lu, P., and Pierson, B. L., "Aircraft Terrain Following Based on a Nonlinear Continuous Predictive Control Approach," *Journal of Guidance, Control, and Dynamics*, Vol. 13, No. 1, 1996, pp. 817–823.

[16]Kaminer, I., Pascoal, A., Hallberg, E., and Silvestre, C., "Trajectory Tracking for Autonomous Vehicles: An Integrated Approach to Guidance and Control," *Journal of Guidance, Control, and Dynamics*, Vol. 21, No. 1, 1998, pp. 29–38.

[17]Lu, P., "Regulation About Time-Varying Trajectories: Precision Entry Guidance Illustrated," *Journal of Guidance, Control, and Dynamics*, Vol. 22, No. 6, 1999, pp. 784–790.

[18]Schierman, J. D., Ward, D. G., Hull, J. R., Monaco, J. F., and Ruth, M. J., "Adaptive Guidance Systems for Hypersonic Reusable Launch Vehicles," *Proceedings of the IEEE Aerospace Conference*, Vol. 6, Inst. of Electrical and Electronics Engineers, Piscataway, NJ, 2001, pp. 2657–2668.

[19]Milam, M. B., Mushambi, K., and Murray, R. M., "A New Computation Approach for Real-Time Trajectory Generation for Constrained Mechanical Systems," *Proceedings of the 39th IEEE Conference on Decision and Control*, Vol. 1, No. 12-15, Inst. of Electrical and Electronics Engineers, Piscataway, NJ, 2000, pp. 845–851.

[20]Verma, A., and Junkins, J. L., "Inverse Dynamics Approach for Real-Time Determination of Feasible Aircraft Reference Trajectories," AIAA Paper 99-4241, Aug. 1999.

[21]Zipfel, P. H., "Squint Angle Guidance for Missiles with SAR Sensors," AIAA Missiles Sciences Conf., Dec. 1996.

[22]Hodgson, J. A., and Lee, D. W., "Terminal Guidance Using a Doppler Beam Sharpening Radar," AIAA Paper 2003-5796, Aug. 2003.

[23]*U.S. Standard Atmosphere 1976*, National Oceanic and Atmospheric Administration, NASA, and U.S. Air Force, U.S. Government Printing Office, Washington, DC, 1976.

[24]Zipfel, P. H., *Modeling and Simulation of Aerospace Vehicle Dynamics*, AIAA Education Series, AIAA, Reston, VA, 2000, pp. 423–426 and 449–451.

[25]Betts, J. T., *Practical Methods for Optimal Control Using Nonlinear Programming*, Advances in Design and Control, Society for Industrial and Applied Mathematics, Philadelphia, 2001.